Neurobiology of Disease 130 (2019) 104532

Contents lists available at ScienceDirect

Neurobiology of Disease

journal homepage: www.elsevier.com/locate/ynbdi

Modified age-dependent expression of NaV1.6 in an ALS model correlates with motor cortex excitability alterations

Luana Saba[a], Maria Teresa Viscomi[b], Alessandro Martini[c], Silvia Caioli[c], Nicola Biagio Mercuri[a,c], Ezia Guatteo[c,d], Cristina Zona[a,c,*]

[a] Department of Systems Medicine, University of Rome "Tor Vergata" via Montpellier 1, Rome 00133, Italy
[b] Università Cattolica del Sacro Cuore, Istituto di Istologia ed Embriologia, Fondazione Policlinico Universitario A. Gemelli, Largo F. Vito 1, Rome 00168, Italy
[c] IRCCS Fondazione Santa Lucia, via del Fosso di Fiorano 64, Rome 00143, Italy
[d] Department of Motor Science and Wellness, University of Naples 'Parthenope', Via Medina 40, Naples 80133, Italy

ARTICLE INFO

Keywords:
ALS
G93A
Electrophysiology
Neuronal excitability
Persistent Na^+ current
NaV1.6
Calcium de-regulation

ABSTRACT

Cortical hyperexcitability is an early and intrinsic feature of Amyotrophic Lateral Sclerosis (ALS), but the mechanisms underlying this critical neuronal dysfunction are poorly understood. Recently, we have demonstrated that layer V pyramidal neurons (PNs) in the primary motor cortex (M1) of one-month old (P30) G93A ALS mice display an early hyperexcitability status compared to Control mice. In order to investigate the time-dependent evolution of the cortical excitability in the G93A ALS model, here we have performed an electrophysiological and immunohistochemical study at three different mouse ages. M1 PNs from 14-days old (P14) G93A mice have shown no excitability alterations, while M1 PNs from 3-months old (P90) G93A mice have shown a hypoexcitability status, compared to Control mice. These age-dependent cortical excitability dysfunctions correlate with a similar time-dependent trend of the persistent sodium current (INa_P) amplitude alterations, suggesting that INa_P may play a crucial role in the G93A cortical excitability aberrations. Specifically, immunohistochemistry experiments have indicated that the expression level of the NaV1.6 channel, one of the voltage-gated Na^+ channels mainly distributed within the central nervous system, varies in G93A primary motor cortex during disease progression, according to the excitability and INa_P alterations, but not in other cortical areas. Microfluorometry experiments, combined with electrophysiological recordings, have verified that P30 G93A PNs hyperexcitability is associated to a greater accumulation of intracellular calcium ($[Ca^{2+}]_i$) compared to Control PNs, and that this difference is still present when G93A and Control PNs fire action potentials at the same frequency.

These results suggest that $[Ca^{2+}]_i$ de-regulation in G93A PNs may contribute to neuronal demise and that the NaV1.6 channels could be a potential therapeutic target to ameliorate ALS disease progression.

1. Introduction

Amyotrophic Lateral Sclerosis (ALS) is a fatal disease of unknown etiology, caused by the progressive degeneration of upper and lower motor neurons (UMNs and LMNs, respectively) (Mathis et al., 2017). The neurodegeneration leads to the progressive failure of the neuromuscular system and inexorably to paralysis and death 3–5 years after disease onset (Hardiman and van den Berg, 2017). ALS may be sporadic (sALS, about 90% of ALS cases) or familial (fALS, about 10% of ALS cases) and, among the genes identified to be implicated in ALS, SOD1 gene (encoding Cu/Zn superoxide dismutase 1) mutations account for 12–20% of fALS cases and 1–7% of sALS cases (Brown, 2017; Kapeli et al., 2017).

Mouse models based on gene abnormalities associated with ALS are a valid tool for investigating the neurobiological basis of the pathology (Van Damme et al., 2017). In particular, the $SOD1^{G93A}$ transgenic mouse (G93A), overexpressing the human $SOD1^{G93A}$ mutation (Gurney, 1994), is the most used and characterized mouse model of ALS

Abbreviations: ALS, Amyotrophic Lateral Sclerosis; UMN, upper motor neuron; LMN, lower motor neuron; sALS, sporadic Amyotrophic Lateral Sclerosis; fALS, familial Amyotrophic Lateral Sclerosis; SOD1, superoxide dismutase 1; INa_p, persistent voltage Na^+ current; NaV, voltage-gated Na^+ channels; CNS, central nervous system; APs, action potentials; AIS, axonal initial segment; M1, primary motor cortex; $[Ca^{2+}]_i$, intracellular calcium concentration; P14, post-natal day 14; P30, post-natal day 30; P90, post-natal day 90

* Corresponding author at: Department of Systems Medicine, University of Rome "Tor Vergata" via Montpellier 1, Rome 00133, Italy.
E-mail address: zona@uniroma2.it (C. Zona).

https://doi.org/10.1016/j.nbd.2019.104532
Received 29 May 2019; Received in revised form 28 June 2019; Accepted 10 July 2019
Available online 11 July 2019
0969-9961/

(Battaglia and Bruno, 2018; Nardo et al., 2016).

Despite the intense research, the etiopathogenetic mechanism of ALS is still obscure and this devastating progressive pathology still lacks an effective cure able to slow down or arrest the ongoing neurodegeneration (Kim et al., 2018; Petrov et al., 2017). To date, the only drugs utilized for ALS treatment are the free radical scavenger edaravone (Radicava), recently approved by the U.S. Food and Drug Administration (FDA) (Rothstein, 2017; Silani, 2017), and Riluzole (Hinchcliffe and Smith, 2017; Mathis et al., 2017), both able to reduce morbidity in ALS, though the mechanism(s) by which they exert their therapeutic effects remain elusive (Jaiswal, 2019). A wide range of possible neural pathways modulated by Riluzole have been postulated, including glutamatergic modulation (Blasco et al., 2014; Lazarevic et al., 2018), down-modulation of the neuronal repetitive firing and inhibition of the persistent voltage-dependent Na^+ current (INa_P) (Carunchio et al., 2010; Geevasinga et al., 2016a; Lamanauskas and Nistri, 2008; Pieri et al., 2009). Specifically, the subthreshold non-inactivating voltage-dependent INa_P is expressed in several neuronal types (Ceballos et al., 2017; Kiss, 2008). This particular current is characterized by a rapid activation and pronounced slow inactivation kinetics, maintaining its activated state for hundreds of milliseconds (Carter et al., 2012). It has been ascertained that INa_P is generated by the same voltage-gated Na^+ channels (NaV_s) sustaining the transient Na^+ current, and that it depends on the interaction between the NaV α- and β-subunits (Aman et al., 2009; Qu et al., 2001). INa_p has a key role in the input signal integration by amplifying dendritic excitatory postsynaptic potentials (Fricker and Miles, 2000; Muller et al., 2018; Vervaeke et al., 2006), and in the neuronal excitability regulation (Kole et al., 2008; Wu et al., 2005) by maintaining neuronal membrane potential near the threshold value and causing spontaneous firing (Ceballos et al., 2017; Raman et al., 2000).

In neurons, action potentials (APs) are generated at the level of the axonal initial segment (AIS) (Kole et al., 2008; Leterrier et al., 2010), a specialized neuronal site characterized by an array of scaffolding proteins (Sobotzik et al., 2009; Yoshimura and Rasband, 2014) and clusters of NaV_s intricately involved in AP generation, conduction, and transition between single spiking and bursting (Hargus et al., 2013; Muller et al., 2018). In mammals, the NaV family is composed of nine members, NaV1.1 to NaV1.9 (Ahern et al., 2016; Catterall, 2012). Among the multiple NaV isoforms expressed within the brain (Candenas et al., 2006; Kress and Mennerick, 2009), the NaV1.6 isoform is the most abundantly expressed in adulthood (Gonzalez-Cabrera et al., 2017). Specifically, NaV1.6 is highly expressed along the AIS (Hu et al., 2009), where it increases repetitive firing rate by reducing the neuronal threshold for AP generation (Gonzalez-Cabrera et al., 2017; Hu et al., 2009; Osorio et al., 2010).

The transcranial magnetic stimulation (TMS) technique in ALS patients has permitted to demonstrate that cortical excitability is aberrantly increased at an early state of the disease, preceding and correlating with development of LMN dysfunction (Vucic and Kiernan, 2013; Vucic and Kiernan, 2017). Moreover, it has been recognized as an early process also in animal models (Carunchio et al., 2010; Ozdinler et al., 2011; Pieri et al., 2009), providing a pathogenic basis for ALS, with corticomotor neuronal hyperexcitability activating the glutamate excitotoxic cascade *via* trans-synaptic mechanism and, subsequently, provoking the motor neuron degeneration (Geevasinga et al., 2016b). In fact, the excessive activation of ionotropic glutamate receptors on the postsynaptic membrane leads to increased $[Ca^{2+}]_i$ and activation of Ca^{2+}-dependent enzymatic pathways, resulting in neuronal death (Geevasinga et al., 2016b). In addition, previous excitability studies in ALS patients have shown that increased INa_p in motor axons induces hyperexcitability (Iwai et al., 2016). Anomalies in the INa_p have been also demonstrated in a zebrafish ALS model (Benedetti et al., 2016) and in primary cortical cultures from G93A mice, strongly indicating an involvement of this current in the cortical hyperexcitability (Pieri et al., 2009).

To date, the mechanisms underlying the development of cortical hyperexcitability in ALS remain to be elucidated, but excessive glutamatergic transmission, dysfunction of NaV_s, hyperactivity of excitatory cortical neurons, as well as degeneration of inhibitory intracortical neurons, all seems to contribute to it (Bae et al., 2013; Menon et al., 2017; Saba et al., 2016).

The data herein reported clearly indicate a non-linear evolution of the cortical excitability in the G93A mice, correlated to a modified NaV1.6 channel expression, suggesting that targeting this channel specifically in the motor cortex might represent an early intervention strategy for counteract ALS progression.

2. Materials and methods

2.1. Animals

The experiments have been performed using B6SJLTgN (SOD1-G93A)1 Gur mice that overexpressed the G93A mutated human SOD1 (G93A) constructed by Gurney (1994), and non-transgenic littermates as Control group. The mice were originally obtained from Jackson Laboratories (Bar Harbor) and then housed in our animal facilities. The presence of the human transgene was evaluated by performing a screening protocol on the mouse tail tips, as previously described (Pieri et al., 2003).

Male mice at P30 and P90 were weighted before the sacrifice for the experimental procedures, using a digital balance (Philips).

Transgenic mice showed signs of hind limb weakness and rapidly developed a paralysis that resembled fALS both clinically and pathologically at 4 months of age and died within 7–14 days (Gurney, 1994).

Procedures involving the animals and their care were carried out in accordance with the ethical guidelines of the European Communities Council Directive (2010/63/EU), Italian laws (D. Lgs 26/2014 art. 31 n.26) and all relevant legislations, and approved by the Ethical Committee for the Protection of Animals in Scientific Research at the Santa Lucia Foundation (approval No. 317-2017-PR). All efforts were made to minimize animal suffering and the number of animals used in this study.

2.2. Slice preparation

Control and G93A male mice, at post-natal day 14 (P14), 30 (P30) and 90 (P90), were anesthetized with isofluorane (Sigma–Aldrich) and decapitated. The brains were removed and placed in cold artificial cerebrospinal fluid solution (ACSF) containing the following (in mM): 126 NaCl, 26 $NaHCO_3$, 2.5 KCl, 1.25 NaH_2PO_4, 2 $MgSO_4$, 2 $CaCl_2$, and 10 glucose, gassed with 95% O_2–5% CO_2 (pH 7.4, 300 mOsm). Coronal slices (275 μm) were obtained as previously described (Saba et al., 2016) using a vibratome (Leica VT1000S), covering approximately from 1.18 mm anterior to the Bregma, to −0.34 mm posterior to the Bregma. Slices were then incubated in the oxygenated ACSF, initially at 37 °C for 45 min and subsequently at room temperature (RT). The single slice was then transferred to a recording chamber and submerged in continuously flowing oxygenated ACSF (31 °C, 2 ml/min) for electrophysiological experiments.

2.3. Electrophysiology

Recordings were obtained on pyramidal neurons (PNs) from the deep part of layer V of the primary motor cortex (M1), which were visually identified using an upright infrared microscope (Axioskop 2 FS), a 40× water immersion objective (Achroplan), and a CCD camera (Cool Snap, Photometrics). Only neurons with a typical large pyramidal-shaped soma, a thick apical dendrite oriented toward the pial surface (Stuart et al., 1993), a regular-spiking, a membrane resistance lower than 100 MΩ, and a membrane capacitance in the range of 75–125 pF, corresponding to a diameter of 16–21 μm (Oswald et al.,

2013; Suter et al., 2013), were considered in this study. Patch-clamp electrodes for electrophysiological whole-cell recordings were made by using borosilicate glass pipettes (outside diameter 1.5 mm), pulled with PP-83 (Narishige, Japan) to obtain a resistance of 3–5 MΩ. After the formation of a high-resistance seal (> 1 GΩ), the capacitance and the resistance of the electrodes were compensated electronically. A Multiclamp 700B patch-clamp amplifier (Molecular Devices) was used to amplify the signals, sampled at 20 KHz, filtered at 3 KHz, and stored in a computer. A Digidata 1440A (Molecular Devices) was used to acquire the data. The "Membrane Test" protocol, consisting of a 5 mV hyperpolarizing step from – 60 mV, at 33.3 Hz, for 30 ms (Krashia et al., 2017), of pClamp 10.4 software (Molecular Devices), was used to obtain the membrane resistance (Rm) for each patched neuron. Whole-cell access resistances measured in the voltage-clamp mode were in the range of 5–20 MΩ.

A current-clamp configuration protocol consisting in 1-s depolarizing current steps (+20/+200 pA, 20 pA step) was used to record the action potential (AP) firings in the M1 layer V PNs. The pipettes were filled with an intracellular solution containing (in mM): 145 KGlu, 1 EGTA, 0.1 $CaCl_2$, 10 HEPES, 2 $MgCl_2$ and 2 Mg-ATP (pH 7.3, 300 mOsm). For each neuron, the firing frequency (number of actions potentials per second) was plotted against the injected currents (F–I relationship).

To record the persistent Na^+ current (INa_p), 4-Aminopyridine (4-AP, 2 mM) and $CdCl_2$ (0.2 mM) were added in the ACSF in order to block K^+ and Ca^{2+} conductances, respectively. The internal solution was as follows (in mM): 130 CsCl, 20 tetraethyl-ammonium-Cl, 1 $MgCl_2$, 0.24 $CaCl_2$, 10 D-glucose, 5 EGTA, 10 HEPES, 2 ATP-Mg (pH 7.3 with CsOH, 300 mOsm). To isolate the INa_p, a slow ramp protocol (from −100 mV to +30 mV; 14 mV/s) in voltage-clamp mode, was used, in order to prevent activation of the fast transient Na^+ current component. When the slow voltage ramp was applied to patched neurons, the recorded currents increased relatively linearly in the sub-threshold region near rest, because of the passive leak current, but at more depolarized levels between −70 and −60 mV, the current usually deviated downward from the extrapolated leak current. The ramp protocol was applied in the absence and after 5 min of Tetrodotoxin (TTX, 1 μM; Tocris) exposure. TTX was added in the ACSF containing 4-Aminopyridine (4-AP, 2 mM) and $CdCl_2$ (0.2 mM), and perfused on slice using a gravity perfusion system. Traces obtained in the presence of TTX were subtracted from those obtained in its absence, to extrapolate the inward current referred to as INa_p.

To test the contribution of NaV1.6 in the INa_p at P30 G93A PNs, we used the TTX metabolite 4,9-anhydro-tetrodotoxin (4,9-ah-TTX, 300 nM; Tocris), a compound which has a greater potency in blocking NaV1.6 channels over other NaV isoforms (Rosker et al., 2007; Teramoto and Yotsu-Yamashita, 2015). INa_p before and after 5 min of 4,9-ah-TTX exposure were recorded, and the percentage of INa_p reduction after the exposure to the NaV1.6 blocker was calculated, in order to obtain the Nav1.6 contribution on total INa_p amplitude.

2.4. Immunofluorescence and densitometric analyses

Mice were anesthetized with Rompun (20 mg ml^{-1}, 0.5 ml kg^{-1}, i.p., Bayer) and Zoletil (100 mg ml^{-1}, 0.5 ml kg^{-1}, Virbac) and perfused transcardially with 50 ml saline followed by 50 ml of 4% paraformaldehyde in phosphate buffer (PB; 0.1 M, pH 7.4). The brains were post-fixed in paraformaldehyde overnight at 4 °C and then immersed in a 30% sucrose solution at 4 °C. The brains were cut into 30 mm-thick coronal sections using a freezing microtome. In order to avoid staining variability, brain sections of Control and G93A mice were concomitantly incubated with the same cocktail of primary and secondary antibodies. Specifically, the sections selected for immunofluorescence were incubated for 48 h with primary antibodies including mouse anti-neuronal nuclei (NeuN; 1:200; Millipore, MAB-377), rabbit anti-NaV1.6 antibody (1:200; Alomone Labs, Israel) prepared in PB containing 0.3% Triton X-100. Each incubation step was followed by three 5-min rinses in PB. Afterwards, sections were incubated 2 h at RT with secondary antibodies including Alexa Fluor 555 donkey anti-rabbit IgG (1:200; Invitrogen), Alexa Fluor 488 donkey anti-mouse IgG (1:200; Invitrogen). Furthermore, the sections were counterstained with NeuroTrace® 640/660 deep-red Fluorescent Nissl Stain (1: 200; Invitrogen) in order to determine the cytoarchitectonic area (primary motor cortex, M1) and layer (layer V) of interest as in Saba et al., 2016. After further washes in PB, the sections were mounted using an anti-fade medium (Fluoromount; Sigma).

The specificity of immunohistochemical labeling of anti-NaV1.6 was confirmed by omission of primary antibodies and use of normal serum instead (negative controls).

Sections were rinsed, mounted, coverslipped and then examined using a confocal laser scanning microscope (Zeiss LSM700, Germany). The confocal image acquisitions were performed using consistent settings for laser power and detector gain.

Quantification of the immunoreactivity (IR) of NaV1.6 in G93A and Control mice was performed off-line on confocal images by densitometric analyses, as already reported (Lo Iacono et al., 2015). Briefly, after background subtraction, the neurons of layer V of M1 and somatosensory cortex (S1) and neurons of layer II-III of M1 NaV1.6-associated signal were quantified by manually outlining individual neurons and measuring cell associated fluorescence intensity with the ImageJ software (http://rsb.info.nih.gov/ij/). The F/A ratio defines mean fluorescence of individual cells (F) normalized to total cellular surface (A). Quantification was done on 150 cells per cortical region/layer per group (n = 5 mice per group), and was conducted blind to the animal's experimental group.

2.5. Electrophysiology combined with microfluorometry

Patch-clamp recordings combined to microfluorometry were performed in a subset of experiments in PNs at P30, according to published procedures (Davoli et al., 2015; Guatteo et al., 2013). PNs from the deep part of layer V of the primary motor cortex (M1) were visually identified using an upright infrared microscope (Olympus, BX51WI) *via* a 40× water immersion objective (Olympus) and a CCD camera (Photometrics, Evolve). Recordings were conducted using a Multiclamp 700B amplifier (Molecular Devices) using pipettes (2–5 MΩ) filled with (mM): 125 K-gluconate, 10 KCl, 0.1 CaCl2, 1 MgCl2, 10 HEPES, 0.75 mM EGTA, 0.25 Fura-2, 2 ATP-Mg^{2+} (pH 7.3, 280 mOsm). Fura-2 loaded neurons were illuminated using a monochromator-based system (Till Photonics) which provided 340 and 380 nm excitation wavelengths. Emitted light passed a barrier filter (440 nm) and was detected by the CCD camera. Images were acquired at 1-second intervals using MetaFluor software. Calcium levels are reported as fluorescence ratios (R) calculated from the formula $(F_{340soma}\text{-}F_{340bg})/(F_{380soma}\text{-}F_{380bg})$ as previously reported (Guatteo et al., 2013) and according to Grynkiewicz et al. (1985). In order to obtain a proper time resolution of fluorescence signals during action potential firing, in this set of experiments we applied long-lasting depolarizing current steps (10 s) of increasing amplitudes (20 to 260 pA, 20 pA increment).

2.6. Statistical analyses

The analysis of current-clamp recordings was performed off-line using the software Clampfit 10.4 (Molecular Devices). The data are presented as the mean ± standard error (SE), with "n" indicating the number of analyzed neurons. At least three mice from each experimental group were used for the measurement of the parameter reported in the Result Section. Statistical analysis was performed using Origin 7 (Microcal Software) and SPSS 17.0 for Windows (SPSS, Inc.) software. Statistically significant differences were determined using the unpaired Student's t-test or One-Way ANOVA followed by Bonferroni's correction. Values of $p < .05$ were considered statistically significant.

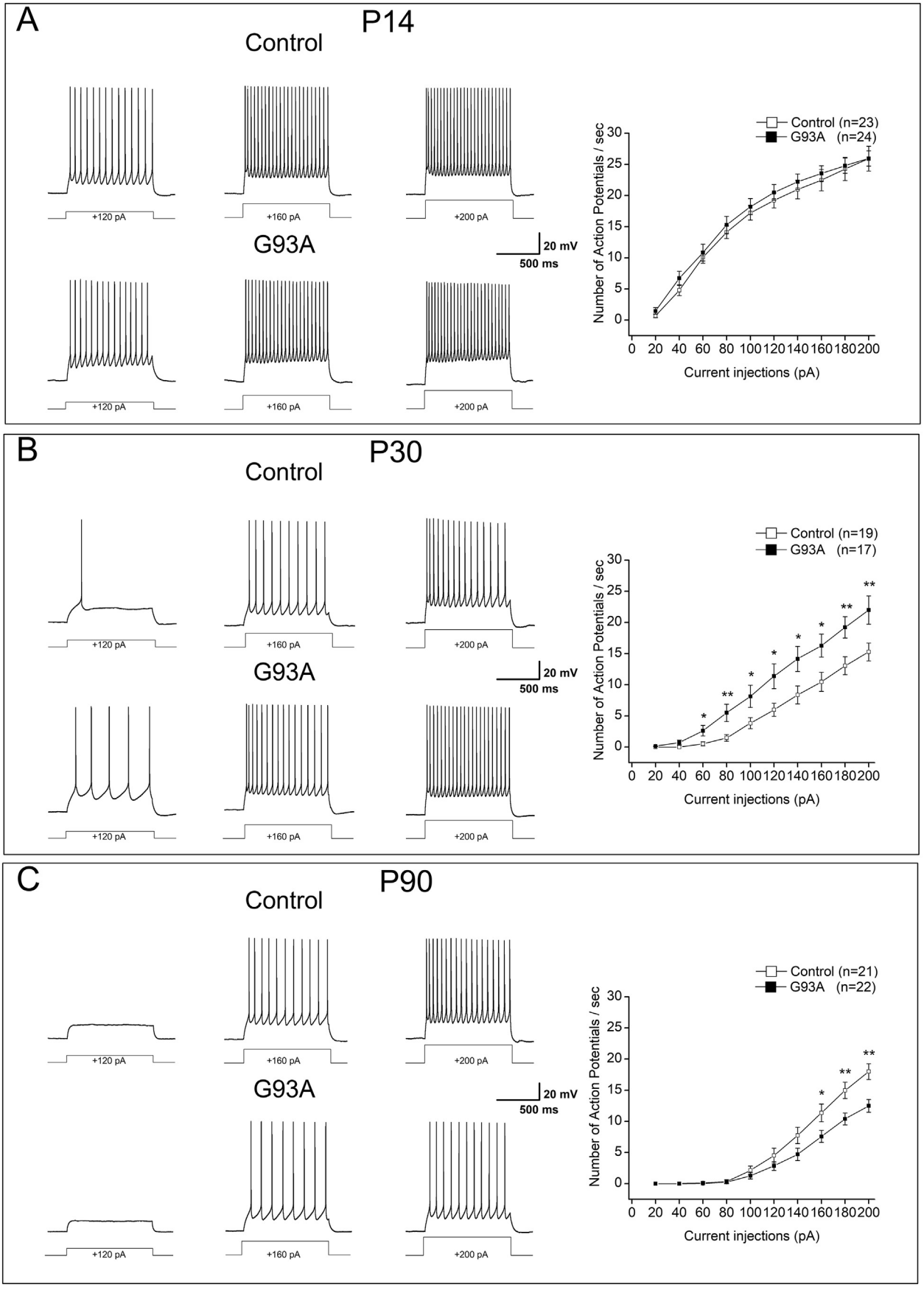

(caption on next page)

Fig. 1. G93A mice show a non-linear evolution of cortical excitability.
(A) Left- Representative repetitive firing recorded from M1 layer V PNs in Control and G93A mice at P14, evoked by +120, +160 and +200 pA current injections (1 s) under the current-clamp condition (Control: Vm = −63 mV; G93A: Vm = −64 mV). **Right-** Means and standard errors of firing frequencies, measured as APs number, plotted against the injected current intensities (+20/+200 pA, 20 pA steps, 1 s) of Control and G93A PNs at P14. The number of APs evoked by the same injected current was not different between the two neuronal populations ($p > .05$; unpaired Student *t*-test). **(B) Left-** Representative repetitive firing recorded from M1 layer V PNs in Control and G93A mice at P30, evoked by +120, +160 and +200 pA current injections (1 s) under the current-clamp condition (Control: Vm = −70 mV; G93A: Vm = −71 mV). **Right-** Means and standard errors of firing frequencies, measured as APs number, plotted against the injected current intensities (+20/+200 pA, 20 pA steps, 1 s) of Control and G93A PNs at P30. Over the range of injected currents, the frequencies of APs varied in Control PNs from 0 to 15.3 ± 1.4 Hz, and in G93A PNs from 0.06 ± 0.06 to 21.9 ± 2.3 Hz (Control: $n = 19$; G93A: $n = 17$). The number of APs evoked by injected currents equal or above +60 pA was significantly higher in G93A neurons compared to Control. *$p < .05$; **$p < .01$ unpaired Student's *t*-test. **(C) Left-** Representative repetitive firing recorded from M1 layer V PNs in Control and G93A mice at P90, evoked by +120, +160 and + 200 pA current injections (1 s) under the current-clamp condition (Control: Vm = − 69 mV; G93A: Vm = − 70 mV). **Right-** Means and standard errors of firing frequencies, measured as APs number, plotted against the injected current intensities (+20/+200 pA, 20 pA steps, 1 s) of Control and G93A PNs at P90. Over the range of injected currents, the frequencies of APs varied in Control PNs from 0 to 18 ± 1.3 Hz, and in G93A PNs from 0 to 12.5 ± 1 Hz (Control: $n = 21$; G93A: $n = 22$). The number of APs evoked by injected currents equal or above +160 pA was lower in G93A neurons compared to Control. *p < .05, **p < .01, unpaired Student's *t*-test.

3. Results

3.1. G93A mice show a non-linear evolution of cortical excitability

In our recent work we have demonstrated in G93A mice at P30, an early presymptomatic stage of the disease, a hyperexcitability status of M1 layer V PNs, compared to Control (Saba et al., 2016). In order to investigate the excitability temporal trend of these neurons, we have performed whole-cell patch-clamp recordings, in current-clamp mode, in Control and G93A mice at P14, P30 and P90. Only neurons that looked like pyramidal and that responded to a current injection with repetitive firing, as reported in Materials and Methods, have been considered for the final analysis.

Results we have obtained indicate that at P14, when mouse motor cortex has not yet reached full maturation (Gonzalez-Lozano et al., 2016; Moyer and Zuo, 2018; Tjia et al., 2017), the AP firing frequencies in response to 1-sec depolarizing current step (+20/+200 pA, 20 pA increment) recorded in Control ($n = 23$) and G93A PNs ($n = 24$) are not significantly different ($p > .05$, Student's *t*-test) (Fig. 1A). Instead, at P30 the recordings confirmed the hyperexcitability status of G93A M1 PNs previously reported (Saba et al., 2016) (Fig. 1B). Recordings from G93A mice at P90, a symptomatic stage of the disease, revealed that at this age M1 PNs display a decreased number of APs respect to Control PNs in response to the same depolarizing current injection, a hallmark of a hypoexcitability status (Control: $n = 21$; G93A: $n = 22$; $p < .05$ for injected currents equal or above +160 pA, unpaired Student's *t*-test) (Fig. 1C).

To verify whether the PN AP firing difference at P30 and P90 was due to different Rm, we have studied the membrane resistance in Control and G93A at all ages. The results obtained indicate that the Rm was similar between Control and G93A mice at all ages ($p > .05$, One Way ANOVA following Bonferroni's correction), suggesting that at P30 and P90 the Rm variations were not involved in the G93A firing aberrations. Interestingly, a decrease in Rm values during mice development (Etherington and Williams, 2011; Maravall et al., 2004), corresponding to a decreased AP firing frequency (Al-Muhtasib et al., 2018; Sun and Harrington, 2019), was observed both in Control and G93A PNs (P14 Control: 222.7 ± 14.1 MΩ, $n = 23$; P14 G93A: 229.9 ± 14.1 MΩ, n = 24; P30 Control: 97.7 ± 5.9 MΩ, $n = 19$; P30 G93A: 109.5 ± 8.8 MΩ, $n = 17$; P90 Control: 90.7 ± 5.6 MΩ, n = 21; P90 G93A: 101.1 ± 4.2 MΩ, $n = 22$. $p < .001$, P14 *vs* P30 and P90 for both groups, One Way ANOVA following Bonferroni's correction).

The body weight was not significantly different between Control and G93A mice at P30 and P90 (P30 Control: 17.4 ± 0.43 g, n = 21; G93A: 16 ± 0.6 g, n = 23; p > .05, Student's *t*-test. P90 Control: 28.1 ± 0.6 g, $n = 15$; G93A: 27.4 ± 0.7 g, $n = 13$; p > .05, Student's *t*-test), in accordance with the results previously reported (Schafer and Hermans, 2011; Weydt et al., 2003).

3.2. Persistent Na^+ current aberrations in M1 layer V pyramidal neurons of G93A mice

Voltage-dependent channels control the neuronal AP firing ability and, among them, the non-inactivating persistent Na^+ current (INa_P) is known to play a key role in facilitating the repetitive firing (Stafstrom, 2007; Yue et al., 2005). To study whether the INa_p properties were altered in M1 layer V PNs G93A mice compared to Control at P14, P30 and P90, we have performed voltage-clamp recordings using a slow ramp protocol (from −100 mV to +30 mV; 14 mV/s) to evoke INa_p current and to prevent activation of the fast-transient Na^+ current component, under experimental conditions in which Ca^{2+} and K^+ currents were pharmacologically blocked (see Materials and Methods). For all tested neurons, the INa_p current-voltage relationship was obtained by subtracting the slow current amplitude before and after TTX perfusion (Fig. 2).

Results we have obtained show that INa_p amplitude, measured at the peak, was not significantly different between Control and G93A PNs at P14 (Control: 57 ± 4.2 pA, n = 19; G93A: 56.7 ± 6.3 pA, $n = 14$; $p > .05$, unpaired Student's *t*-test) (Fig. 2A), whereas at P30 the mean INa_p peak amplitude was significantly higher in G93A PNs (359 ± 47.7 pA, $n = 27$) compared to Control PNs (234 ± 35 pA, n = 23; $p < .05$, unpaired Student's *t*-test) (Fig. 2B). By contrast, at P90 the INa_p mean amplitude was significantly lower in G93A PNs (198 ± 23 pA, n = 22) compared to Control PNs (289 ± 36.7 pA, n = 17; p < .05, unpaired Student's *t*-test) (Fig. 2C), indicating a time-dependent aberration in the INa_p, as detected for firing frequency. The INa_p threshold potential and peak potential were not significantly different between Control and G93A PNs, at any age analyzed (data not shown).

3.3. Altered NaV1.6 expression level in G93A M1 layer V

The Na^+ channel isoform Nav1.6, encoded by the *SCN8A* gene, is highly localized along the axonal initial segment and is known to contribute in INa_p generation and, consequently, to play a central role in regulating the neuronal firing pattern (Gonzalez-Cabrera et al., 2017; Hu et al., 2009; Osorio et al., 2010).

To determine whether changes in INa_p amplitude observed between Control and G93A mice at different ages reflect a different expression level of the NaV1.6 channel protein, we have performed immunofluorescence and densitometric analyses on cerebral cortex of Control and G93A mice at P14, P30 and P90 (Fig. 3).

Immunofluorescent labeling of M1 with anti-NaV1.6 antibody showed intense labelling in all layers, in both the Control and G93A mice at all the time points considered. In particular, cell bodies of PNs of layer V were clearly labeled and the NaV1.6 staining appeared to be cytoplasmic (Fig. 3).

Densitometric analysis of NaV1.6 immunoreactivity (IR) in M1 cortical layer V showed that the NaV1.6 expression level was similar in

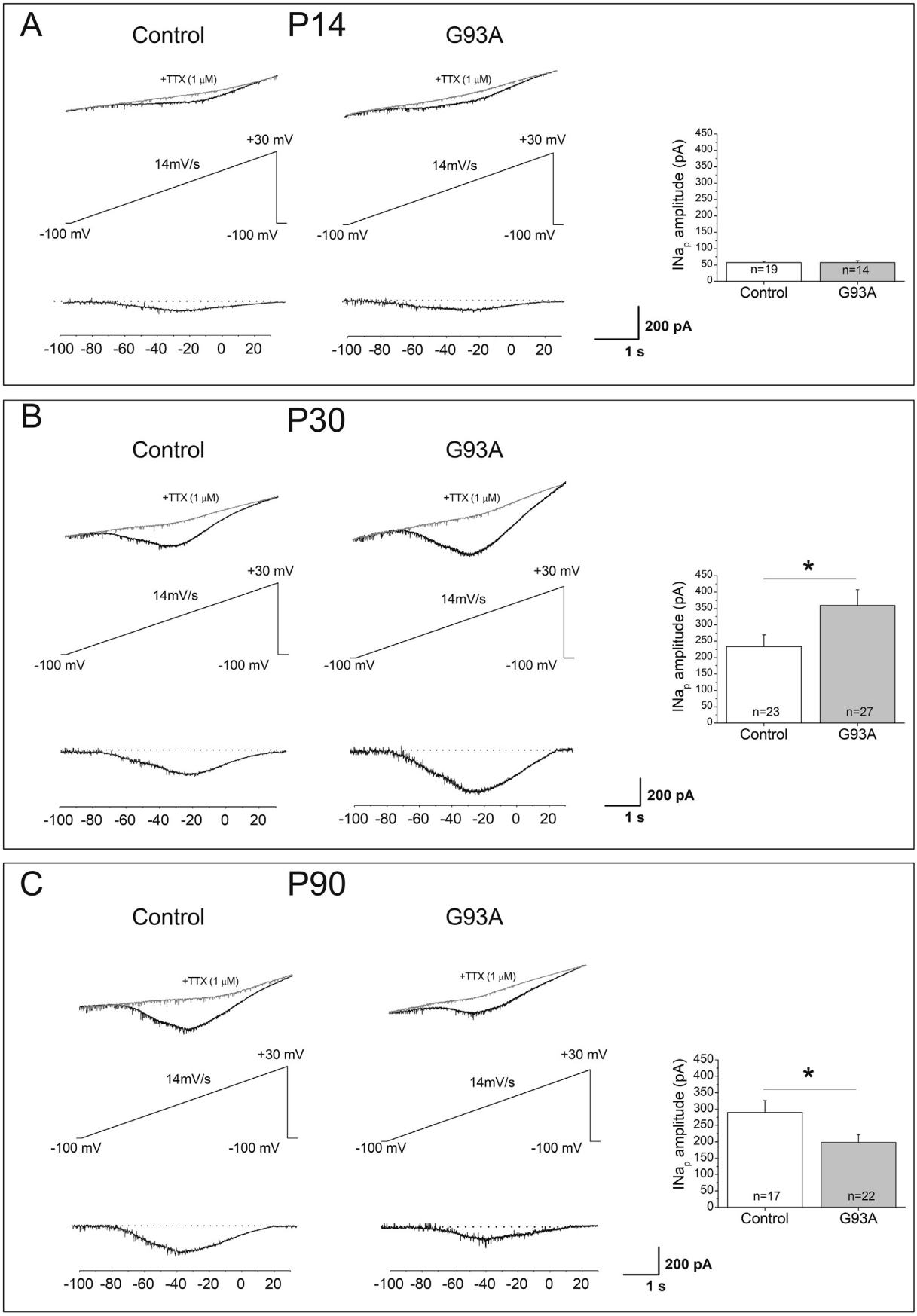

(caption on next page)

Fig. 2. Persistent Na^+ current alterations in M1 layer V PNs during G93A mouse development.
(A) Left- Persistent Na^+ current (INa_p) evoked by a slow voltage ramp protocol (14 mV/s from −100 to +30 mV) in M1 layer V PNs from Control and G93A at P14. The current traces shown at the bottom of the panel were obtained by digitally subtracting the traces recorded in 1 μM TTX (grey) from initial recordings (black). **Right-** Bar plot of mean values with standard errors of INa_p current amplitude in P14 Control and G93A PNs. The values related to INa_p current amplitude resulted no significantly different between Control and G93A neurons. $p > .05$ unpaired Student *t*-test.
(B) Left- INa_p evoked by a slow voltage ramp protocol (14 mV/s from −100 to +30 mV) in M1 layer V PNs from Control and G93A at P30. The current traces shown at the bottom of the panel were obtained by digitally subtracting the traces recorded in 1 μM TTX from initial recordings. **Right-** Bar plot of mean values with standard errors of INa_p current amplitude in P30 Control and G93A PNs. The values related to INa_p current amplitude resulted significantly higher in G93A neurons compared to Control. *$p < .05$, unpaired Student's *t*-test.
(C) Left- INa_p evoked by a slow voltage ramp protocol (14 mV/s from −100 to +30 mV) in Control and G93A M1 layer V PNs at P90. The current traces shown at the bottom of the panel were obtained by digitally subtracting the traces recorded in 1 μM TTX (grey) from initial recordings (black). **Right-** Bar plot of mean values with standard errors of INa_p current amplitude in P90 Control and G93A PNs. The values related to INa_p current amplitude resulted significantly lower in G93A neurons compared to Control. *$p < .05$, unpaired Student *t*-test.

Control and G93A PNs at P14 (Control: F/A = 10.66 ± 0.24; G93A: F/A = 11.06 ± 0.34; $p > .05$, unpaired Student's *t*-test) (Fig. 3C). At P30 our findings showed that the NaV1.6 expression level was significantly increased in G93A (F/A = 13.73 ± 0.20) compared to Control PNs (F/A = 10.32 ± 0.27; $p < .001$, unpaired Student's *t*-test) (Fig. 3F). Conversely, at P90, the NaV1.6 expression level was significantly lower in G93A (F/A = 10.44 ± 0.58) compared to Control PNs (F/A = 12.91 ± 0.46; $p < .001$, unpaired Student's *t*-test) (Fig. 3I).

To be sure that these findings are M1-layer V-specific, we analyzed the expression pattern of NaV1.6 in somatosensory cortex (S1) and in M1 layer II-III neurons. Densitometric analysis of NaV1.6 IR in S1 cortical layer V, as well as in M1 layer II-III, showed that in both regions the NaV1.6 expression level was similar in Control and G93A at all the time points analyzed (Suppl. F1), confirming that the different expression level of NaV1.6 protein observed between Control and G93A mice is M1-layer V-specific.

3.4. The NaV1.6 channel plays a role in the increased INa_p of M1 layer V PNs from P30 G93A mice

To investigate the NaV1.6 contribution on the total INa_p amplitude, we have tested the effect of 4,9-anhydrotetrodotoxin (4,9-ah-TTX; 300 nM), a potent NaV1.6 blocker (Rosker et al., 2007; Teramoto and Yotsu-Yamashita, 2015), on INa_p of M1 layer V PNs in G93A and Control mice at P30.

By using the previously described ramp protocol, we have calculated for each neuron the percentage of the INa_p reduction following

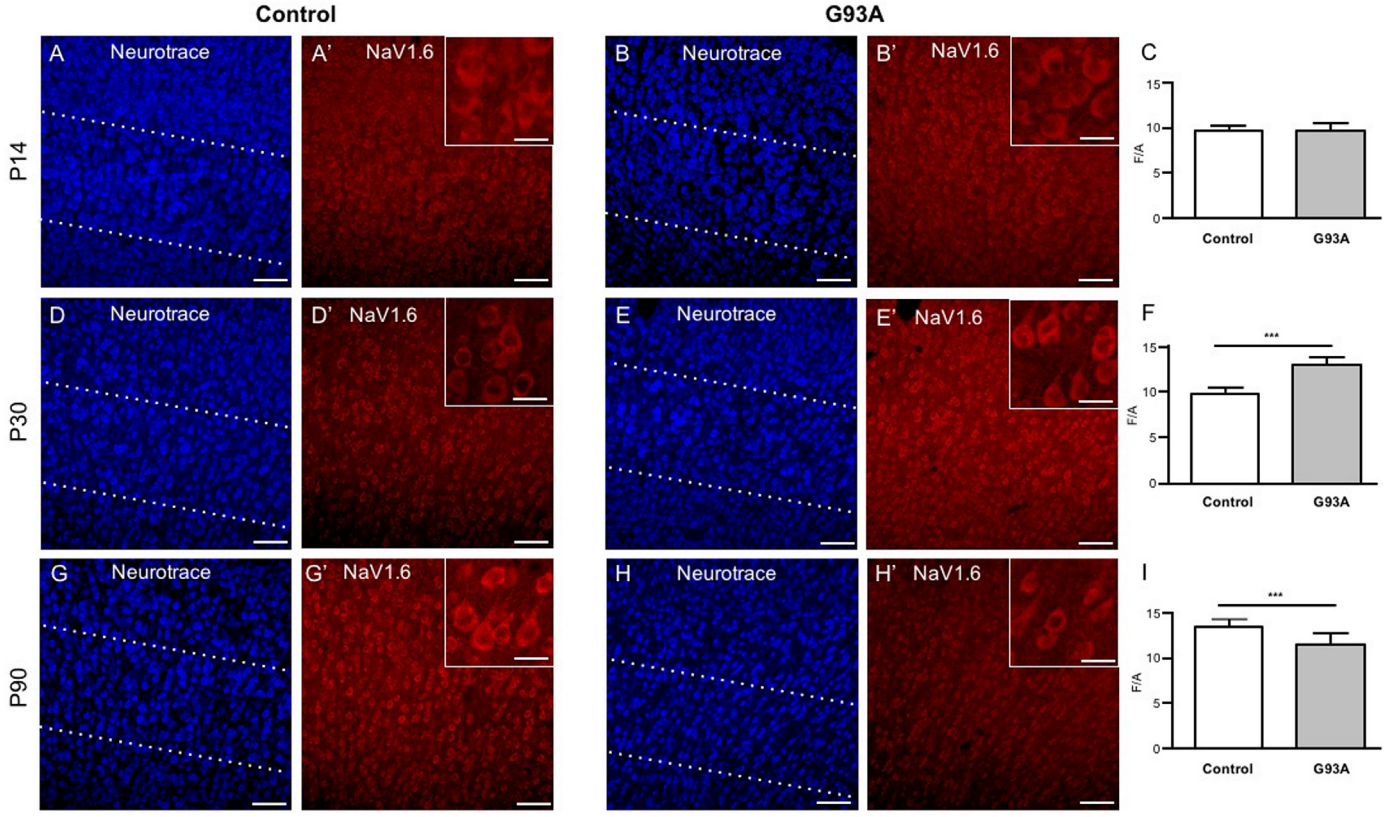

Fig. 3. Altered NaV1.6 immunoreactivity in G93A M1.
Immunofluorescence of NaV1.6 in layer V of motor cortex of Control and G93A mice at P14, P30 and P90. Confocal images of double immunofluorescence for Neurotrace (blue **A, B, D, E, G, H**) and NaV1.6 (red **A′, B′, D′, E′, G′, H′**) showing the different NaV1.6 expression (insets) in neurons of layer V between the two experimental groups at the different ages considered. **(C, F and I)** Histograms of densitometric values of NaV1.6 in neurons of layer V of motor cortex of Control and G93A mice at the different ages considered, expressed as mean fluorescence of individual cells, normalized to total cellular surface (F/A; $N = 150$ cells/group; 5 mice/group). Scale bars: (A–B′, D–E′, G–H′) = 100 μm; insets = 10 μm. ***$p < .001$, unpaired Student *t*-test. (For interpretation of the references to colour in this figure legend, the reader is referred to the web version of this article.)

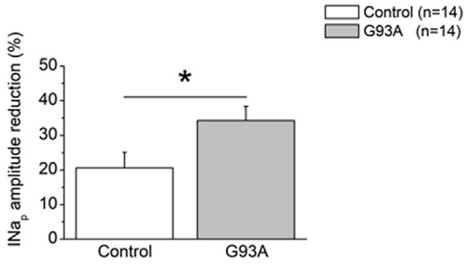

Fig. 4. NaV1.6 contribution in IN_{ap} is higher in G93A M1 layer V PNs than Controls from P30 aged mice.
Bar plot of mean values with standard errors related to the % reduction of INap amplitude after the exposure to 4,9-ah-TTX (300 nM), the NaV1.6 channel blocker, of M1 layer V PNs in Control and G93A mice at P30. The INa_p current reduction following 4,9-ah-TTX perfusion resulted significantly higher in G93A PNs compared to Control PNs, suggesting an increased contribution of NaV1.6 in INa_p. *p < .05, unpaired Student *t*-test.

5 minutes 4,9-ah-TTX perfusion (300 nM; (Hargus et al., 2013). The INa_p current reduction following 4,9-ah-TTX perfusion resulted significantly higher in G93A PNs compared to Control (Control: 20.6% ± 4.5; $n = 14$; G93A: 34.3% ± 4; n = 14; $p < .05$, unpaired Student's *t*-test) (Fig. 4), clearly indicating that the contribution of NaV1.6 to INa_p amplitude is significantly higher in G93A compared to Control.

3.5. Calcium imaging

To explore if the hyperexcitability status of M1 layer V PNs from G93A mice at P30 correlated with a de-regulation of Ca^{2+} homeostasis, we have performed a subset of experiments in which electrophysiological recordings were combined to microfluorometry, both in G93A and Control PNs (Fig. 5).

Basal Ca^{2+} concentration levels, measured at the resting membrane potential, in the absence of any stimulus, was significantly higher in G93A (0.44 ± 0.024 R, $n = 17$) in comparison with Control PNs (0.39 ± 0.009 R, $n = 19$, p < .05, unpaired Student's *t*-test; Fig. 5A). We have confirmed that G93A PNs were in a hyperexcitability status also in this experimental set in which we applied 10 s duration depolarizing current steps (see Material and Method section), as their firing frequency was significantly higher than in Control PNs, at all stimulus intensities ($p = .001$, unpaired Student's *t*-test; Fig. 5B). Accordingly, the extent of $[Ca^{2+}]_i$ accumulation in response to depolarizing currents was greater in G93A respect to Control PNs, at all stimulus intensities (p < .05, unpaired Student's *t*-test; Fig. 5C, D). To test whether the observed $[Ca^{2+}]_i$ accumulation is associated with changes in release and/or reuptake kinetics, we have analyzed rise and decay times of the calcium transient evoked by 260 pA current injection (Fig. 5C, rectangle). We have found that these values were similar in the two neuronal populations (Rise time Control: 4.94 ± 0.31 s, $n = 12$; G93A: 5.49 ± 0.41 s, $n = 13$, $p > .05$; T_{100} Control: 25.11 ± 4.25 s, n = 12; G93A: 26.02 ± 3.46 s, n = 13, p > .05, unpaired Student's *t*-test; Fig. 5E,F). Moreover, we have compared $[Ca^{2+}]_i$ levels between G93A and Control PNs firing at the same frequency, independently on the stimulus intensity (Fig. 5G). The two curves overlapped in the lower firing frequency ranges (from 0 to 2.9 Hz to 9–11.9 Hz, p < .05, unpaired Student's *t*-test), but significantly differed above 12 Hz (12–14.9 Hz and 15–17.9 Hz, p < .05, unpaired Student's *t*-test), suggesting that mechanisms other than the voltage-gated Ca^{2+} channels are responsible for aberrant $[Ca^{2+}]_i$ accumulation in G93A PNs.

4. Discussion

The phenomenon of cortical hyperexcitability has been widely described in sporadic and familial ALS patients (Geevasinga et al., 2016b; Vucic et al., 2008; Williams et al., 2013), and in animal models (Carunchio et al., 2010; Naka and Mills, 2000; Nieto-Gonzalez et al., 2011; Pieri et al., 2009; Zanette et al., 2002). Interestingly, Transcranial Magnetic Stimulation (TMS) studies on ALS patients have revealed that cortical hyperexcitability appears at an early state of the disease (Geevasinga et al., 2016b; Vucic and Kiernan, 2017), and that survival is inversely correlated with the degree of this cortical abnormal excitability (Kanai et al., 2012; Shibuya et al., 2016). The alterations of cortical electrical properties in the G93A ALS mouse model have been recently demonstrated by our research group, associated to the increased glutamatergic synaptic transmission and to the neuronal morphological aberrations, all occurring at an early disease phase (Saba et al., 2016). The increased action potential firing frequency and excitatory neurotransmission of the primary motor neuron would provoke the excitotoxicity phenomenon, leading to an exacerbated calcium influx into the postsynaptic motor neuron, which may trigger the motor neuron degeneration typical of this pathology (Dong et al., 2009; Patai et al., 2017). Riluzole, one of the drugs utilized for the treatment of ALS, inhibits glutamatergic neurotransmission (Blasco et al., 2014; Lazarevic et al., 2018) and normalizes cortical excitability (Carunchio et al., 2010; Geevasinga et al., 2016a; Lamanauskas and Nistri, 2008; Pieri et al., 2009), indicating that these electrical alterations can be considered among the pathological mechanisms occurring in ALS.

To date, a factor that has been given little attention is the role that postnatal maturation processes have in the development of the disease. Although many studies have demonstrated the cortical hyperexcitability in the G93A mouse, it is not known when it firstly manifests, as well as how it evolves during the disease progression. To this aim, in this study we have answered to these unresolved questions. Specifically, we have performed experiments on the G93A ALS mouse model at three different ages, reflecting three different stages of the disease progression. The G93A age of 14 post-natal days (P14) is considered asymptomatic because any degeneration sign is detectable (Fogarty et al., 2015; van Zundert et al., 2008). The G93A P30 age is considered the early symptomatic phase, with aberrant cortical excitability, glutamatergic neurotransmission, neuronal morphology and degeneration (Ozdinler et al., 2011; Saba et al., 2016; Weydt et al., 2003), while the G93A P90 age corresponds to the symptomatic phase, characterized by the gradual motor neuronal degeneration, motor deficits and muscle weakness (Jara et al., 2012; Ozdinler et al., 2011; Spalloni et al., 2011; Steyn et al., 2013). Our results have demonstrated the presence of bidirectional changes in G93A cortical excitability across mouse development. In fact, while at P14, the G93A M1 PNs firing frequency is not significantly different than Control, it significantly increases at P30, and significantly reduces at P90.

The non-linear altered cortical excitability in ALS mouse model has been also reported previously, although with a different evolution (Kim et al., 2017). Instead, studies performed on induced pluripotent stem cell-derived motor neurons from ALS patients harboring the *C9orf72*, the *TARDP43*, the *fused-in-sarcoma* and the *SOD1* ALS-causing mutations, agree with our results. Specifically, independently from genotype, patient-derived motor neurons show, at an early stage in culture, a status of hyperexcitability (Kiskinis et al., 2014; Wainger et al., 2014), followed by a status of hypoexcitability after many days *in vitro* (Devlin et al., 2015; Guo et al., 2017; Naujock et al., 2016).

Voltage-dependent sodium currents are crucial in the control of neuronal excitability and, specifically, the persistent sodium current (INa_p) plays a key role in modulating membrane excitability (Doeser et al., 2014; Stafstrom, 2007). The pivotal role of INa_p in the ALS cortical hyperexcitability has been already reported by our research group and by others (Benedetti et al., 2016; Carunchio et al., 2010; Geevasinga et al., 2015; Pieri et al., 2009) but, to our knowledge, its correlation with the lower action potential frequency we have observed at P90 has never been reported. For this reason, we have analyzed this specific current at the three mouse ages. Results we have herein obtained suggest that INa_p is a major factor influencing cortical

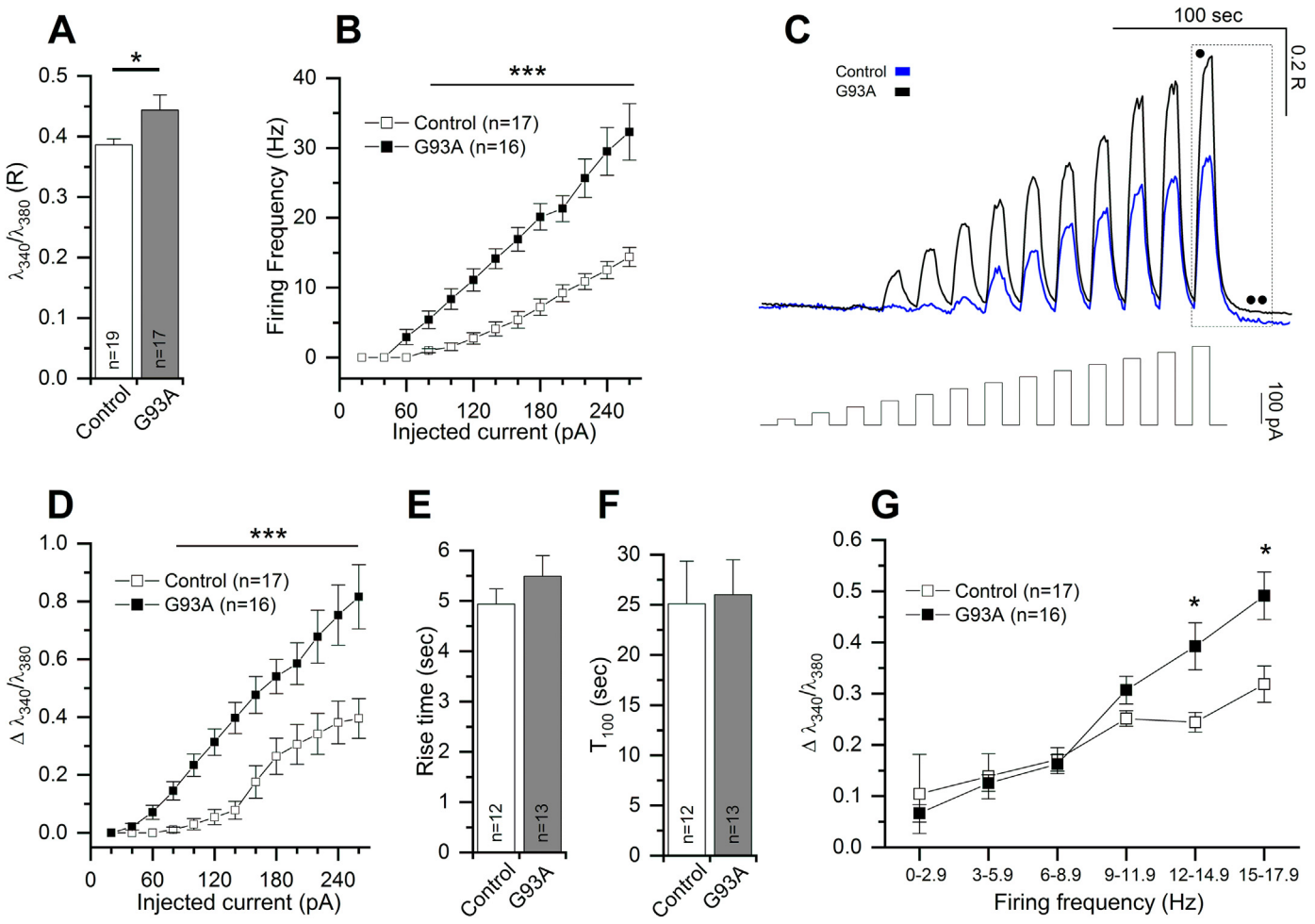

Fig. 5. Analysis of baseline and stimulated intracellular $[Ca^{2+}]_i$ in M1 layer V PNs of P30 Control and G93A mice.
A) Mean values of basal intracellular $[Ca^{2+}]$ in M1 layer V PNs of Control and G93A mice. **B)** Firing frequency plotted against injected current. **C)** Depolarizing current steps from +20 pA to +260 pA (20 pA increment, 10 s, *bottom*) stimulate intracellular $[Ca^{2+}]$ elevation in M1 layer V PNs of both Control and G93A mice (*top*). The baseline levels of two traces have been superimposed to better appreciate the amplitude of Ca^{2+} signals in Control and G93A PNs. Rise (●) and decay (●●) times of the $[Ca^{2+}]_i$ elevation at last current step (+260 pA) were analyzed in both genotypes. **D)** Stimulated intracellular $[Ca^{2+}]_i$ elevations are plotted against injected currents. **E–F)** Mean values of rise time and decay time (T_{100}) of the $[Ca^{2+}]_i$ elevation at last current step. **G)** Stimulated intracellular $[Ca^{2+}]_i$ elevations are plotted against firing frequency ranges (3 Hz) in both Control and G93A mice. *p < .05, ***p < .001, unpaired Student's *t*-test.

excitability: it is elevated months before G93A symptoms onset, in parallel to the neuronal hyperexcitability, and it is reduced during the symptomatic phase, in parallel to the neuronal hypoexcitability, compared to Control PNs from mice at the same age. Since it is known that a small increase of INa_p can dramatically facilitate hyperexcitability, the role of the persistent sodium current in ALS is an interesting focus to investigate.

The INa_p cortical alterations have been widely described in neurological deficits as epilepsy because this current can maintain the membrane depolarization for a long time, generating the epilepticus firing (Chen et al., 2011; Doeser et al., 2014). Indeed, specific sodium channel mutations have been associated with INa_p increase and epilepsy syndromes (Patino and Isom, 2010; Stafstrom, 2007).

INa_p is induced by the activation of several types of voltage-dependent sodium channels (Nav1.1–1.9) (Lin and Baines, 2015; Stafstrom, 2007) and, among them, the Nav1.6 is critically involved in the neuronal excitability control due to its specific localization within the Axonal Initial Segment (AIS) (Hu et al., 2009; Katz et al., 2018). Mutations in the gene codifying for the Nav1.6 channel, the *SCN8A* gene, and alterations in the channel expression level are reported both in humans and in murine models of epilepsy (Blumenfeld et al., 2009; Veeramah et al., 2012; Wagnon et al., 2016). A decrease of the NaV1.6 level significantly reduces the neuronal spontaneous firing and the frequencies of evoked-firing in many neurons (Makinson et al., 2014; Royeck et al., 2008; Van Wart and Matthews, 2006). Furthermore, the deletion of Nav1.6 encoding gene, the *SCN8A* gene, reduces neuronal electrical activity and firing (Osorio et al., 2010; Raman et al., 1997), and causes mouse paralysis (Burgess et al., 1995). Conversely, aberrant overexpression of the NaV1.6 channel increases INa_p, confirming its critical role in controlling neuronal excitability (Lopez-Santiago et al., 2017; Wong et al., 2018).

To date, there are no data in the literature reporting a direct involvement of NaV1.6 in the pathogenesis of ALS and, for this reason, we have studied the expression level of this sodium channel subtype during disease progression. Our results indicate that the bidirectional alterations of the INa_p are coupled to the parallel tissue- and layer-specific increase and decrease of the NaV1.6 expression level, suggesting a pivotal role of this sodium channel subtype in the development of the time-dependent G93A cortical functional aberrations. Moreover, in G93A M1 PNs at P30 the Nav1.6 contribution to the INap amplitude was significantly higher than in Control, confirming the pivotal role of this specific channel in the early cortical hyperexcitability.

Abnormal intrinsic neuronal repetitive firing has been proposed very early on to cause glutamate-mediated excitotoxicity and neuronal degeneration in ALS (Rothstein et al., 1990), with an excessive intracellular calcium elevation and apoptotic death (Ilieva et al., 2009;

Kuo et al., 2005; von Lewinski and Keller, 2005). Interestingly, our data show that M1 PNs from G93A at P30, among being hyperexcitable, have a significant higher cytoplasmic Ca^{2+} concentration already at their resting membrane potential compared to Control PNs, suggesting that both the intrinsic neuronal hyperexcitability and increased excitatory neurotransmission would put neuron in a more excitotoxic-susceptible state. Accordingly, in G93A PNs the extent of $[Ca^{2+}]_i$ accumulation in response to depolarizing currents was greater, at all stimulus intensities, but this alteration was not merely due to the G93A PNs higher firing frequency. In fact, by comparing $[Ca^{2+}]_i$ levels between G93A and Control PNs firing at the same frequency, we have observed that at high firing frequencies, independently from the intensity of the current stimulus, the G93A $[Ca^{2+}]_i$ level was significantly higher than Control. This result leads us to speculate that other mechanisms than those expected, as the more intense recruitment of voltage-gated calcium channels upon increasing firing frequencies, are responsible for $[Ca^{2+}]_i$ accumulation in G93A PNs. Several studies have linked deregulation of Ca^{2+} homeostasis and neuron degeneration occurring in neurodegenerative diseases including ALS (recently reviewed by (Czell et al., 2017). Ca^{2+} deregulation is multifactorial, possibly involving excess of extracellular glutamate (van der Spek et al., 2018), abnormal recovery following AMPA receptor activation (Guatteo et al., 2007), loss of Ca^{2+}-binding proteins (Esanov et al., 2017; Moloney et al., 2017) and mitochondria Ca^{2+} overload which results in chronic mitochondria depolarization (Langseth et al., 2017). Additionally, dysfunction of plasma membrane extrusion mechanisms, including Ca^{2+}-ATPase and Na^+/Ca^{2+} exchanger (Anzilotti et al., 2018), may also contribute to Ca^{2+} deregulation in cortical PNs of this mouse model of ALS.

In this study we provide evidence that cortical excitability alterations during G93A disease progression follow a non-linear trend, matching with specific INa_p and NaV1.6 aberrations. Moreover, the early hyperexcitability status of G93A pyramidal neurons (PNs) is accompanied to $[Ca^{2+}]_i$ de-regulation.

5. Conclusions

In conclusion, results obtained in this study not only contribute improving the knowledge on ALS pathology, but could provide new molecular and pharmacological therapeutic strategies effective in blocking, or slowing down, the progression of the disease. In fact, the identification of a new target, such as the NaV1.6 voltage-dependent sodium channel, could lead to design new experimental strategies able to modulate its expression level and activity. This would allow to contrast the temporal evolution of cortical dysfunctions in the mouse model of ALS and thus slow down the progression of the disease.

Supplementary data to this article can be found online at https://doi.org/10.1016/j.nbd.2019.104532.

Funding

This research has been funded by University of Rome “Tor Vergata” (CUP E82I15001060005) and by AriSLA Foundation, “HyperALS” project.

Author disclosure statement

The authors declare that no competing financial interests exist.

Declaration of Competing Interest

None.

References

Ahern, C.A., Payandeh, J., Bosmans, F., Chanda, B., 2016. The hitchhiker's guide to the voltage-gated sodium channel galaxy. J. Gen. Physiol. 147, 1–24. https://doi.org/10.1085/jgp.201511492.

Al-Muhtasib, N., Forcelli, P.A., Vicini, S., 2018. Differential electrophysiological properties of D1 and D2 spiny projection neurons in the mouse nucleus accumbens core. Phys. Rep. 6, e13784. https://doi.org/10.14814/phy2.13784.

Aman, T.K., Grieco-Calub, T.M., Chen, C., Rusconi, R., Slat, E.A., Isom, L.L., Raman, I.M., 2009. Regulation of persistent Na current by interactions between beta subunits of voltage-gated Na channels. J. Neurosci. 29, 2027–2042. https://doi.org/10.1523/JNEUROSCI.4531-08.2009.

Anzilotti, S., Brancaccio, P., Simeone, G., Valsecchi, V., Vinciguerra, A., Secondo, A., Petrozziello, T., Guida, N., Sirabella, R., Cuomo, O., Cepparulo, P., Herchuelz, A., Amoroso, S., Di Renzo, G., Annunziato, L., Pignataro, G., 2018. Preconditioning, induced by sub-toxic dose of the neurotoxin L-BMAA, delays ALS progression in mice and prevents Na(+)/Ca(2+) exchanger 3 downregulation. Cell Death Dis. 9, 206. https://doi.org/10.1038/s41419-017-0227-9.

Bae, J.S., Simon, N.G., Menon, P., Vucic, S., Kiernan, M.C., 2013. The puzzling case of hyperexcitability in amyotrophic lateral sclerosis. J. Clin. Neurol. 9, 65–74. https://doi.org/10.3988/jcn.2013.9.2.65.

Battaglia, G., Bruno, V., 2018. Metabotropic glutamate receptor involvement in the pathophysiology of amyotrophic lateral sclerosis: new potential drug targets for therapeutic applications. Curr. Opin. Pharmacol. 38, 65–71. https://doi.org/10.1016/j.coph.2018.02.007.

Benedetti, L., Ghilardi, A., Rottoli, E., De Maglie, M., Prosperi, L., Perego, C., Baruscotti, M., Bucchi, A., Del Giacco, L., Francolini, M., 2016. INaP selective inhibition reverts precocious inter- and motorneurons hyperexcitability in the Sod1-G93R zebrafish ALS model. Sci. Rep. 6, 24515. https://doi.org/10.1038/srep24515.

Blasco, H., Mavel, S., Corcia, P., Gordon, P.H., 2014. The glutamate hypothesis in ALS: pathophysiology and drug development. Curr. Med. Chem. 21, 3551–3575 (doi:CMC-EPUB-62359).

Blumenfeld, H., Lampert, A., Klein, J.P., Mission, J., Chen, M.C., Rivera, M., Dib-Hajj, S., Brennan, A.R., Hains, B.C., Waxman, S.G., 2009. Role of hippocampal sodium channel Nav1.6 in kindling epileptogenesis. Epilepsia. 50, 44–55. https://doi.org/10.1111/j.1528-1167.2008.01710.x.

Brown, C., 2017. Non-familial ALS: a tangled web. Nature. 550, S109–S111. https://doi.org/10.1038/550S109a.

Burgess, D.L., Kohrman, D.C., Galt, J., Plummer, N.W., Jones, J.M., Spear, B., Meisler, M.H., 1995. Mutation of a new sodium channel gene, Scn8a, in the mouse mutant 'motor endplate disease'. Nat. Genet. 10, 461–465. https://doi.org/10.1038/ng0895-461.

Candenas, L., Seda, M., Noheda, P., Buschmann, H., Cintado, C.G., Martin, J.D., Pinto, F.M., 2006. Molecular diversity of voltage-gated sodium channel alpha and beta subunit mRNAs in human tissues. Eur. J. Pharmacol. 541, 9–16. https://doi.org/10.1016/j.ejphar.2006.04.025.

Carter, B.C., Giessel, A.J., Sabatini, B.L., Bean, B.P., 2012. Transient sodium current at subthreshold voltages: activation by EPSP waveforms. Neuron. 75, 1081–1093. https://doi.org/10.1016/j.neuron.2012.08.033.

Carunchio, I., Curcio, L., Pieri, M., Pica, F., Caioli, S., Viscomi, M.T., Molinari, M., Canu, N., Bernardi, G., Zona, C., 2010. Increased levels of p70S6 phosphorylation in the G93A mouse model of Amyotrophic Lateral Sclerosis and in valine-exposed cortical neurons in culture. Exp. Neurol. 226, 218–230. https://doi.org/10.1016/j.expneurol.2010.08.033.

Catterall, W.A., 2012. Sodium Channel Mutations and Epilepsy. (doi:NBK98185 [book-accession]).

Ceballos, C.C., Roque, A.C., Leao, R.M., 2017. A negative slope conductance of the persistent sodium current prolongs subthreshold depolarizations. Biophys. J. 113, 2207–2217. https://doi.org/10.1016/j.bpj.2017.06.047.

Chen, S., Su, H., Yue, C., Remy, S., Royeck, M., Sochivko, D., Opitz, T., Beck, H., Yaari, Y., 2011. An increase in persistent sodium current contributes to intrinsic neuronal bursting after status epilepticus. J. Neurophysiol. 105, 117–129. https://doi.org/10.1152/jn.00184.2010.

Czell, D., Sapp, P.C., Neuwirth, C., Weber, M., Andersen, P.M., Brown, R.H., 2017. Further analysis of KIFAP3 gene in ALS patients from Switzerland and Sweden. Amyotroph. Lateral Scler. Frontotemporal Degener. 18, 302–304. https://doi.org/10.1080/21678421.2017.1280509.

Davoli, A., Greco, V., Spalloni, A., Guatteo, E., Neri, C., Rizzo, G.R., Cordella, A., Romigi, A., Cortese, C., Bernardini, S., Sarchielli, P., Cardaioli, G., Calabresi, P., Mercuri, N.B., Urbani, A., Longone, P., 2015. Evidence of hydrogen sulfide involvement in amyotrophic lateral sclerosis. Ann. Neurol. 77, 697–709. https://doi.org/10.1002/ana.24372.

Devlin, A.C., Burr, K., Borooah, S., Foster, J.D., Cleary, E.M., Geti, I., Vallier, L., Shaw, C.E., Chandran, S., Miles, G.B., 2015. Human iPSC-derived motoneurons harbouring TARDBP or C9ORF72 ALS mutations are dysfunctional despite maintaining viability. Nat. Commun. 6, 5999. https://doi.org/10.1038/ncomms6999.

Doeser, A., Soares-da-Silva, P., Beck, H., Uebachs, M., 2014. The effects of eslicarbazepine on persistent Na(+) current and the role of the Na(+) channel beta subunits. Epilepsy Res. 108, 202–211. https://doi.org/10.1016/j.eplepsyres.2013.11.022.

Dong, H.W., Heinbockel, T., Hamilton, K.A., Hayar, A., Ennis, M., 2009. Metabotropic glutamate receptors and dendrodendritic synapses in the main olfactory bulb. Ann. N. Y. Acad. Sci. 1170, 224–238. https://doi.org/10.1111/j.1749-6632.2009.03891.x.

Esanov, R., Cabrera, G.T., Andrade, N.S., Gendron, T.F., Brown Jr., R.H., Benatar, M., Wahlestedt, C., Mueller, C., Zeier, Z., 2017. A C9ORF72 BAC mouse model recapitulates key epigenetic perturbations of ALS/FTD. Mol. Neurodegener. 12, 46. https://doi.org/10.1186/s13024-017-0185-9.

Etherington, S.J., Williams, S.R., 2011. Postnatal development of intrinsic and synaptic properties transforms signaling in the layer 5 excitatory neural network of the visual cortex. J. Neurosci. 31, 9526–9537. https://doi.org/10.1523/JNEUROSCI.0458-11.2011.

Fogarty, M.J., Noakes, P.G., Bellingham, M.C., 2015. Motor cortex layer V pyramidal neurons exhibit dendritic regression, spine loss, and increased synaptic excitation in the presymptomatic hSOD1(G93A) mouse model of amyotrophic lateral sclerosis. J.

Neurosci. 35, 643–647. https://doi.org/10.1523/JNEUROSCI.3483-14.2015.
Fricker, D., Miles, R., 2000. EPSP amplification and the precision of spike timing in hippocampal neurons. Neuron. 28, 559–569 (doi:S0896-6273(00)00133-1 [pii]).
Geevasinga, N., Menon, P., Howells, J., Nicholson, G.A., Kiernan, M.C., Vucic, S., 2015. Axonal ion channel dysfunction in c9orf72 familial amyotrophic lateral sclerosis. JAMA Neurol. 72, 49–57. https://doi.org/10.1001/jamaneurol.2014.2940.
Geevasinga, N., Menon, P., Ng, K., Van Den Bos, M., Byth, K., Kiernan, M.C., Vucic, S., 2016a. Riluzole exerts transient modulating effects on cortical and axonal hyperexcitability in ALS. Amyotroph. Lateral Scler. Frontotemporal Degener. 17, 580–588. https://doi.org/10.1080/21678421.2016.1188961.
Geevasinga, N., Menon, P., Ozdinler, P.H., Kiernan, M.C., Vucic, S., 2016b. Pathophysiological and diagnostic implications of cortical dysfunction in ALS. Nat. Rev. Neurol. 12, 651–661. https://doi.org/10.1038/nrneurol.2016.140.
Gonzalez-Cabrera, C., Meza, R., Ulloa, L., Merino-Sepulveda, P., Luco, V., Sanhueza, A., Onate-Ponce, A., Bolam, J.P., Henny, P., 2017. Characterization of the axon initial segment of mice substantia nigra dopaminergic neurons. J. Comp. Neurol. 525, 3529–3542. https://doi.org/10.1002/cne.24288.
Gonzalez-Lozano, M.A., Klemmer, P., Gebuis, T., Hassan, C., van Nierop, P., van Kesteren, R.E., Smit, A.B., Li, K.W., 2016. Dynamics of the mouse brain cortical synaptic proteome during postnatal brain development. Sci. Rep. 6, 35456. https://doi.org/10.1038/srep35456.
Grynkiewicz, G., Poenie, M., Tsien, R.Y., 1985. A new generation of Ca2+ indicators with greatly improved fluorescence properties. J. Biol. Chem. 260, 3440–3450.
Guatteo, E., Carunchio, I., Pieri, M., Albo, F., Canu, N., Mercuri, N.B., Zona, C., 2007. Altered calcium homeostasis in motor neurons following AMPA receptor but not voltage-dependent calcium channels' activation in a genetic model of amyotrophic lateral sclerosis. Neurobiol. Dis. 28, 90–100. https://doi.org/10.1016/j.nbd.2007.07.002.
Guatteo, E., Yee, A., McKearney, J., Cucchiaroni, M.L., Armogida, M., Berretta, N., Mercuri, N.B., Lipski, J., 2013. Dual effects of L-DOPA on nigral dopaminergic neurons. Exp. Neurol. 247, 582–594. https://doi.org/10.1016/j.expneurol.2013.02.009.
Guo, W., Fumagalli, L., Prior, R., Van Den Bosch, L., 2017. Current advances and limitations in modeling ALS/FTD in a dish using induced pluripotent stem cells. Front. Neurosci. 11, 671. https://doi.org/10.3389/fnins.2017.00671.
Gurney, M.E., 1994. Transgenic-mouse model of amyotrophic lateral sclerosis. N. Engl. J. Med. 331, 1721–1722.
Hardiman, O., van den Berg, L.H., 2017. Edaravone: a new treatment for ALS on the horizon? Lancet Neurol. 16, 490–491. https://doi.org/10.1016/S1474-4422(17)30163-1.
Hargus, N.J., Nigam, A., Bertram 3rd, E.H., Patel, M.K., 2013. Evidence for a role of Nav1.6 in facilitating increases in neuronal hyperexcitability during epileptogenesis. J. Neurophysiol. 110, 1144–1157. https://doi.org/10.1152/jn.00383.2013.
Hinchcliffe, M., Smith, A., 2017. Riluzole: real-world evidence supports significant extension of median survival times in patients with amyotrophic lateral sclerosis. Degener Neurol. Neuromuscul. Dis. 7, 61–70. https://doi.org/10.2147/DNND.S135748.
Hu, W., Tian, C., Li, T., Yang, M., Hou, H., Shu, Y., 2009. Distinct contributions of Na(v)1.6 and Na(v)1.2 in action potential initiation and backpropagation. Nat. Neurosci. 12, 996–1002. https://doi.org/10.1038/nn.2359.
Ilieva, H., Polymenidou, M., Cleveland, D.W., 2009. Non-cell autonomous toxicity in neurodegenerative disorders: ALS and beyond. J. Cell Biol. 187, 761–772. https://doi.org/10.1083/jcb.200908164.
Iwai, Y., Shibuya, K., Misawa, S., Sekiguchi, Y., Watanabe, K., Amino, H., Kuwabara, S., 2016. Axonal dysfunction precedes motor neuronal death in amyotrophic lateral sclerosis. PLoS One 11, e0158596. https://doi.org/10.1371/journal.pone.0158596.
Jaiswal, M.K., 2019. Riluzole and edaravone: a tale of two amyotrophic lateral sclerosis drugs. Med. Res. Rev. 39, 733–748. https://doi.org/10.1002/med.21528.
Jara, J.H., Villa, S.R., Khan, N.A., Bohn, M.C., Ozdinler, P.H., 2012. AAV2 mediated retrograde transduction of corticospinal motor neurons reveals initial and selective apical dendrite degeneration in ALS. Neurobiol. Dis. 47, 174–183. https://doi.org/10.1016/j.nbd.2012.03.036.
Kanai, K., Shibuya, K., Sato, Y., Misawa, S., Nasu, S., Sekiguchi, Y., Mitsuma, S., Isose, S., Fujimaki, Y., Ohmori, S., Koga, S., Kuwabara, S., 2012. Motor axonal excitability properties are strong predictors for survival in amyotrophic lateral sclerosis. J. Neurol. Neurosurg. Psychiatry 83, 734–738. https://doi.org/10.1136/jnnp-2011-301782.
Kapeli, K., Martinez, F.J., Yeo, G.W., 2017. Genetic mutations in RNA-binding proteins and their roles in ALS. Hum. Genet. 136, 1193–1214. https://doi.org/10.1007/s00439-017-1830-7.
Katz, E., Stoler, O., Scheller, A., Khrapunsky, Y., Goebbels, S., Kirchhoff, F., Gutnick, M.J., Wolf, F., Fleidervish, I.A., 2018. Role of sodium channel subtype in action potential generation by neocortical pyramidal neurons. Proc. Natl. Acad. Sci. U. S. A. 115, E7184–E7192. https://doi.org/10.1073/pnas.1720493115.
Kim, J., Hughes, E.G., Shetty, A.S., Arlotta, P., Goff, L.A., Bergles, D.E., Brown, S.P., 2017. Changes in the excitability of neocortical neurons in a mouse model of amyotrophic lateral sclerosis are not specific to corticospinal neurons and are modulated by advancing disease. J. Neurosci. 37, 9037–9053. https://doi.org/10.1523/JNEUROSCI.0811-17.2017.
Kim, S.H., Oh, K.W., Jin, H.K., Bae, J.S., 2018. Immune inflammatory modulation as a potential therapeutic strategy of stem cell therapy for ALS and neurodegenerative diseases. BMB Rep. 51, 545–546 (doi:4398 [pii]).
Kiskinis, E., Sandoe, J., Williams, L.A., Boulting, G.L., Moccia, R., Wainger, B.J., Han, S., Peng, T., Thams, S., Mikkilineni, S., Mellin, C., Merkle, F.T., Davis-Dusenbery, B.N., Ziller, M., Oakley, D., Ichida, J., Di Costanzo, S., Atwater, N., Maeder, M.L., Goodwin, M.J., Nemesh, J., Handsaker, R.E., Paull, D., Noggle, S., McCarroll, S.A., Joung, J.K., Woolf, C.J., Brown, R.H., Eggan, K., 2014. Pathways disrupted in human ALS motor neurons identified through genetic correction of mutant SOD1. Cell Stem Cell 14, 781–795. https://doi.org/10.1016/j.stem.2014.03.004.
Kiss, T., 2008. Persistent Na-channels: origin and function. A review. Acta Biol. Hung. 59 (Suppl), 1–12. https://doi.org/10.1556/ABiol.59.2008.Suppl.1.
Kole, M.H., Ilschner, S.U., Kampa, B.M., Williams, S.R., Ruben, P.C., Stuart, G.J., 2008. Action potential generation requires a high sodium channel density in the axon initial segment. Nat. Neurosci. 11, 178–186. https://doi.org/10.1038/nn2040.
Krashia, P., Martini, A., Nobili, A., Aversa, D., D'Amelio, M., Berretta, N., Guatteo, E., Mercuri, N.B., 2017. On the properties of identified dopaminergic neurons in the mouse substantia nigra and ventral tegmental area. Eur. J. Neurosci. 45, 92–105. https://doi.org/10.1111/ejn.13364.
Kress, G.J., Mennerick, S., 2009. Action potential initiation and propagation: upstream influences on neurotransmission. Neuroscience. 158, 211–222. https://doi.org/10.1016/j.neuroscience.2008.03.021.
Kuo, J.J., Siddique, T., Fu, R., Heckman, C.J., 2005. Increased persistent Na(+) current and its effect on excitability in motoneurones cultured from mutant SOD1 mice. J. Physiol. 563, 843–854. https://doi.org/10.1113/jphysiol.2004.074138.
Lamanauskas, N., Nistri, A., 2008. Riluzole blocks persistent Na+ and Ca2+ currents and modulates release of glutamate via presynaptic NMDA receptors on neonatal rat hypoglossal motoneurons in vitro. Eur. J. Neurosci. 27, 2501–2514. https://doi.org/10.1111/j.1460-9568.2008.06211.x.
Langseth, A.J., Kim, J., Ugolino, J.E., Shah, Y., Hwang, H.Y., Wang, J., Bergles, D.E., Brown, S.P., 2017. Cell-type specific differences in promoter activity of the ALS-linked C9orf72 mouse ortholog. Sci. Rep. 7, 5685. https://doi.org/10.1038/s41598-017-05864-2.
Lazarevic, V., Yang, Y., Ivanova, D., Fejtova, A., Svenningsson, P., 2018. Riluzole attenuates the efficacy of glutamatergic transmission by interfering with the size of the readily releasable neurotransmitter pool. Neuropharmacology. 143, 38–48. https://doi.org/10.1016/j.neuropharm.2018.09.021.
Leterrier, C., Brachet, A., Fache, M.P., Dargent, B., 2010. Voltage-gated sodium channel organization in neurons: protein interactions and trafficking pathways. Neurosci. Lett. 486, 92–100. https://doi.org/10.1016/j.neulet.2010.08.079.
von Lewinski, F., Keller, B.U., 2005. Ca2+, mitochondria and selective motoneuron vulnerability: implications for ALS. Trends Neurosci. 28, 494–500. https://doi.org/10.1016/j.tins.2005.07.001.
Lin, W.H., Baines, R.A., 2015. Regulation of membrane excitability: a convergence on voltage-gated sodium conductance. Mol. Neurobiol. 51, 57–67. https://doi.org/10.1007/s12035-014-8674-0.
Lo Iacono, L., Visco-Comandini, F., Valzania, A., Viscomi, M.T., Coviello, M., Giampa, A., Roscini, L., Bisicchia, E., Siracusano, A., Troisi, A., Puglisi-Allegra, S., Carola, V., 2015. Adversity in childhood and depression: linked through SIRT1. Transl. Psychiatry 5, e629. https://doi.org/10.1038/tp.2015.125.
Lopez-Santiago, L.F., Yuan, Y., Wagnon, J.L., Hull, J.M., Frasier, C.R., O'Malley, H.A., Meisler, M.H., Isom, L.L., 2017. Neuronal hyperexcitability in a mouse model of SCN8A epileptic encephalopathy. Proc. Natl. Acad. Sci. U. S. A. 114, 2383–2388. https://doi.org/10.1073/pnas.1616821114.
Makinson, C.D., Tanaka, B.S., Lamar, T., Goldin, A.L., Escayg, A., 2014. Role of the hippocampus in Nav1.6 (Scn8a) mediated seizure resistance. Neurobiol. Dis. 68, 16–25. https://doi.org/10.1016/j.nbd.2014.03.014.
Maravall, M., Stern, E.A., Svoboda, K., 2004. Development of intrinsic properties and excitability of layer 2/3 pyramidal neurons during a critical period for sensory maps in rat barrel cortex. J. Neurophysiol. 92, 144–156. https://doi.org/10.1152/jn.00598.2003.
Mathis, S., Couratier, P., Julian, A., Vallat, J.M., Corcia, P., Le Masson, G., 2017. Management and therapeutic perspectives in amyotrophic lateral sclerosis. Expert. Rev. Neurother. 17, 263–276. https://doi.org/10.1080/14737175.2016.1227705.
Menon, P., Geevasinga, N., van den Bos, M., Yiannikas, C., Kiernan, M.C., Vucic, S., 2017. Cortical hyperexcitability and disease spread in amyotrophic lateral sclerosis. Eur. J. Neurol. 24, 816–824. https://doi.org/10.1111/ene.13295.
Moloney, C., Rayaprolu, S., Howard, J., Fromholt, S., Brown, H., Collins, M., Cabrera, M., Duffy, C., Siemienski, Z., Miller, D., Swanson, M.S., Notterpek, L., Borchelt, D.R., Lewis, J., 2017. Retraction note: transgenic mice overexpressing the ALS-linked protein Matrin 3 develop a profound muscle phenotype. Acta Neuropathol. Commun. 5, 97. https://doi.org/10.1186/s40478-017-0502-0.
Moyer, C.E., Zuo, Y., 2018. Cortical dendritic spine development and plasticity: insights from in vivo imaging. Curr. Opin. Neurobiol. 53, 76–82. https://doi.org/10.1016/j.conb.2018.06.002.
Muller, P., Draguhn, A., Egorov, A.V., 2018. Persistent sodium current modulates axonal excitability in CA1 pyramidal neurons. J. Neurochem. 146, 446–458. https://doi.org/10.1111/jnc.14479.
Naka, D., Mills, K.R., 2000. Further evidence for corticomotor hyperexcitability in amyotrophic lateral sclerosis. Muscle Nerve 23, 1044–1050. https://doi.org/10.1002/1097-4598(200007)23:7<1044::AID-MUS6>3.0.CO;2-Q. (pii).
Nardo, G., Trolese, M.C., Tortarolo, M., Vallarola, A., Freschi, M., Pasetto, L., Bonetto, V., Bendotti, C., 2016. New insights on the mechanisms of disease course variability in ALS from mutant SOD1 mouse models. Brain Pathol. 26, 237–247. https://doi.org/10.1111/bpa.12351.
Naujock, M., Stanslowsky, N., Bufler, S., Naumann, M., Reinhardt, P., Sterneckert, J., Kefalakes, E., Kassebaum, C., Bursch, F., Lojewski, X., Storch, A., Frickenhaus, M., Boeckers, T.M., Putz, S., Demestre, M., Liebau, S., Klingenstein, M., Ludolph, A.C., Dengler, R., Kim, K.S., Hermann, A., Wegner, F., Petri, S., 2016. 4-Aminopyridine induced activity rescues hypoexcitable motor neurons from amyotrophic lateral sclerosis patient-derived induced pluripotent stem cells. Stem Cells 34, 1563–1575. https://doi.org/10.1002/stem.2354.
Nieto-Gonzalez, J.L., Moser, J., Lauritzen, M., Schmitt-John, T., Jensen, K., 2011. Reduced GABAergic inhibition explains cortical hyperexcitability in the wobbler mouse model of ALS. Cereb. Cortex 21, 625–635. https://doi.org/10.1093/cercor/bhq134.
Osorio, N., Cathala, L., Meisler, M.H., Crest, M., Magistretti, J., Delmas, P., 2010. Persistent Nav1.6 current at axon initial segments tunes spike timing of cerebellar granule cells. J. Physiol. 588, 651–670. https://doi.org/10.1113/jphysiol.2010.183798.
Oswald, M.J., Tantirigama, M.L., Sonntag, I., Hughes, S.M., Empson, R.M., 2013. Diversity of layer 5 projection neurons in the mouse motor cortex. Front. Cell.

Neurosci. 7, 174. https://doi.org/10.3389/fncel.2013.00174.
Ozdinler, P.H., Benn, S., Yamamoto, T.H., Guzel, M., Brown Jr., R.H., Macklis, J.D., 2011. Corticospinal motor neurons and related subcerebral projection neurons undergo early and specific neurodegeneration in hSOD1G(9)(3)A transgenic ALS mice. J. Neurosci. 31, 4166–4177. https://doi.org/10.1523/JNEUROSCI.4184-10.2011.
Patai, R., Nogradi, B., Engelhardt, J.I., Siklos, L., 2017. Calcium in the pathomechanism of amyotrophic lateral sclerosis - taking center stage? Biochem. Biophys. Res. Commun. 483, 1031–1039. https://doi.org/10.1016/j.bbrc.2016.08.089.
Patino, G.A., Isom, L.L., 2010. Electrophysiology and beyond: multiple roles of Na+ channel beta subunits in development and disease. Neurosci. Lett. 486, 53–59. https://doi.org/10.1016/j.neulet.2010.06.050.
Petrov, D., Mansfield, C., Moussy, A., Hermine, O., 2017. ALS clinical trials review: 20 years of failure. Are we any closer to registering a new treatment? Front. Aging Neurosci. 9, 68. https://doi.org/10.3389/fnagi.2017.00068.
Pieri, M., Albo, F., Gaetti, C., Spalloni, A., Bengtson, C.P., Longone, P., Cavalcanti, S., Zona, C., 2003. Altered excitability of motor neurons in a transgenic mouse model of familial amyotrophic lateral sclerosis. Neurosci. Lett. 351, 153–156.
Pieri, M., Carunchio, I., Curcio, L., Mercuri, N.B., Zona, C., 2009. Increased persistent sodium current determines cortical hyperexcitability in a genetic model of amyotrophic lateral sclerosis. Exp. Neurol. 215, 368–379. https://doi.org/10.1016/j.expneurol.2008.11.002.
Qu, Y., Curtis, R., Lawson, D., Gilbride, K., Ge, P., DiStefano, P.S., Silos-Santiago, I., Catterall, W.A., Scheuer, T., 2001. Differential modulation of sodium channel gating and persistent sodium currents by the beta1, beta2, and beta3 subunits. Mol. Cell. Neurosci. 18, 570–580. https://doi.org/10.1006/mcne.2001.1039.
Raman, I.M., Sprunger, L.K., Meisler, M.H., Bean, B.P., 1997. Altered subthreshold sodium currents and disrupted firing patterns in Purkinje neurons of Scn8a mutant mice. Neuron. 19, 881–891 (doi:S0896-6273(00)80969-1 [pii]).
Raman, I.M., Gustafson, A.E., Padgett, D., 2000. Ionic currents and spontaneous firing in neurons isolated from the cerebellar nuclei. J. Neurosci. 20, 9004–9016 (doi:20/24/9004 [pii]).
Rosker, C., Lohberger, B., Hofer, D., Steinecker, B., Quasthoff, S., Schreibmayer, W., 2007. The TTX metabolite 4,9-anhydro-TTX is a highly specific blocker of the Na(v1.6) voltage-dependent sodium channel. Am. J. Phys. Cell Physiol. 293, C783–C789. https://doi.org/10.1152/ajpcell.00070.2007.
Rothstein, J.D., 2017. Edaravone: a new drug approved for ALS. Cell. 171, 725. doi:S0092-8674(17)31198-4 [pii]. https://doi.org/10.1016/j.cell.2017.10.011.
Rothstein, J.D., Tsai, G., Kuncl, R.W., Clawson, L., Cornblath, D.R., Drachman, D.B., Pestronk, A., Stauch, B.L., Coyle, J.T., 1990. Abnormal excitatory amino acid metabolism in amyotrophic lateral sclerosis. Ann. Neurol. 28, 18–25. https://doi.org/10.1002/ana.410280106.
Royeck, M., Horstmann, M.T., Remy, S., Reitze, M., Yaari, Y., Beck, H., 2008. Role of axonal NaV1.6 sodium channels in action potential initiation of CA1 pyramidal neurons. J. Neurophysiol. 100, 2361–2380. https://doi.org/10.1152/jn.90332.2008.
Saba, L., Viscomi, M.T., Caioli, S., Pignataro, A., Bisicchia, E., Pieri, M., Molinari, M., Ammassari-Teule, M., Zona, C., 2016. Altered functionality, morphology, and vesicular glutamate transporter expression of cortical motor neurons from a presymptomatic mouse model of amyotrophic lateral sclerosis. Cereb. Cortex 26, 1512–1528. https://doi.org/10.1093/cercor/bhu317.
Schafer, S., Hermans, E., 2011. Reassessment of motor-behavioural test analyses enables the detection of early disease-onset in a transgenic mouse model of amyotrophic lateral sclerosis. Behav. Brain Res. 225, 7–14. https://doi.org/10.1016/j.bbr.2011.06.019.
Shibuya, K., Park, S.B., Geevasinga, N., Menon, P., Howells, J., Simon, N.G., Huynh, W., Noto, Y., Gotz, J., Kril, J.J., Ittner, L.M., Hodges, J., Halliday, G., Vucic, S., Kiernan, M.C., 2016. Motor cortical function determines prognosis in sporadic ALS. Neurology. 87, 513–520. https://doi.org/10.1212/WNL.0000000000002912.
Silani, V., 2017. Therapy in Amyotrophic Lateral Sclerosis (ALS): an unexpected evolving scenario. Arch. Ital. Biol. 155, 118–130. https://doi.org/10.12871/00039829201747.
Sobotzik, J.M., Sie, J.M., Politi, C., Del Turco, D., Bennett, V., Deller, T., Schultz, C., 2009. AnkyrinG is required to maintain axo-dendritic polarity in vivo. Proc. Natl. Acad. Sci. U. S. A. 106, 17564–17569. https://doi.org/10.1073/pnas.0909267106.
Spalloni, A., Origlia, N., Sgobio, C., Trabalza, A., Nutini, M., Berretta, N., Bernardi, G., Domenici, L., Ammassari-Teule, M., Longone, P., 2011. Postsynaptic alteration of NR2A subunit and defective autophosphorylation of alphaCaMKII at threonine-286 contribute to abnormal plasticity and morphology of upper motor neurons in presymptomatic SOD1G93A mice, a murine model for amyotrophic lateral sclerosis. Cereb. Cortex 21, 796–805. https://doi.org/10.1093/cercor/bhq152.
van der Spek, R.A., van Rheenen, W., Pulit, S.L., Kenna, K.P., Ticozzi, N., Kooyman, M., McLaughlin, R.L., Moisse, M., van Eijk, K.R., van Vugt, J., Iacoangeli, A., Andersen, P., Nazli Basak, A., Blair, I., de Carvalho, M., Chio, A., Corcia, P., Couratier, P., Drory, V.E., Glass, J.D., Hardiman, O., Mora, J.S., Morrison, K.E., Mitne-Neto, M., Robberecht, W., Shaw, P.J., Panades, M.P., van Damme, P., Silani, V., Gotkine, M., Weber, M., van Es, M.A., Landers, J.E., Al-Chalabi, A., van den Berg, L.H., Veldink, J.H., 2018. Reconsidering the causality of TIA1 mutations in ALS. Amyotroph. Lateral Scler. Frontotemporal Degener. 19, 1–3. https://doi.org/10.1080/21678421.2017.1413118.
Stafstrom, C.E., 2007. Persistent sodium current and its role in epilepsy. Epilepsy Curr. 7, 15–22. https://doi.org/10.1111/j.1535-7511.2007.00156.x.
Steyn, F.J., Lee, K., Fogarty, M.J., Veldhuis, J.D., McCombe, P.A., Bellingham, M.C., Ngo, S.T., Chen, C., 2013. Growth hormone secretion is correlated with neuromuscular innervation rather than motor neuron number in early-symptomatic male amyotrophic lateral sclerosis mice. Endocrinology. 154, 4695–4706. https://doi.org/10.1210/en.2013-1570.
Stuart, G.J., Dodt, H.U., Sakmann, B., 1993. Patch-clamp recordings from the soma and dendrites of neurons in brain slices using infrared video microscopy. Pflugers Arch. 423, 511–518.
Sun, J., Harrington, M.A., 2019. The alteration of intrinsic excitability and synaptic transmission in lumbar spinal motor neurons and interneurons of severe spinal muscular atrophy mice. Front. Cell. Neurosci. 13, 15. https://doi.org/10.3389/fncel.2019.00015.
Suter, B.A., Migliore, M., Shepherd, G.M., 2013. Intrinsic electrophysiology of mouse corticospinal neurons: a class-specific triad of spike-related properties. Cereb. Cortex 23, 1965–1977. https://doi.org/10.1093/cercor/bhs184.
Teramoto, N., Yotsu-Yamashita, M., 2015. Selective blocking effects of 4,9-anhydrotetrodotoxin, purified from a crude mixture of tetrodotoxin analogues, on NaV1.6 channels and its chemical aspects. Mar. Drugs. 13, 984–995. https://doi.org/10.3390/md13020984.
Tjia, M., Yu, X., Jammu, L.S., Lu, J., Zuo, Y., 2017. Pyramidal neurons in different cortical layers exhibit distinct dynamics and plasticity of apical dendritic spines. Front. Neural Circuits. 11, 43. https://doi.org/10.3389/fncir.2017.00043.
Van Damme, P., Robberecht, W., Van Den Bosch, L., 2017. Modelling amyotrophic lateral sclerosis: progress and possibilities. Dis. Model. Mech. 10, 537–549. https://doi.org/10.1242/dmm.029058.
Van Wart, A., Matthews, G., 2006. Impaired firing and cell-specific compensation in neurons lacking nav1.6 sodium channels. J. Neurosci. 26, 7172–7180. https://doi.org/10.1523/JNEUROSCI.1101-06.2006.
Veeramah, K.R., O'Brien, J.E., Meisler, M.H., Cheng, X., Dib-Hajj, S.D., Waxman, S.G., Talwar, D., Girirajan, S., Eichler, E.E., Restifo, L.L., Erickson, R.P., Hammer, M.F., 2012. De novo pathogenic SCN8A mutation identified by whole-genome sequencing of a family quartet affected by infantile epileptic encephalopathy and SUDEP. Am. J. Hum. Genet. 90, 502–510. https://doi.org/10.1016/j.ajhg.2012.01.006.
Vervaeke, K., Hu, H., Graham, L.J., Storm, J.F., 2006. Contrasting effects of the persistent Na+ current on neuronal excitability and spike timing. Neuron. 49, 257–270. https://doi.org/10.1016/j.neuron.2005.12.022.
Vucic, S., Kiernan, M.C., 2013. Utility of transcranial magnetic stimulation in delineating amyotrophic lateral sclerosis pathophysiology. Handb. Clin. Neurol. 116, 561–575. https://doi.org/10.1016/B978-0-444-53497-2.00045-0.
Vucic, S., Kiernan, M.C., 2017. Transcranial magnetic stimulation for the assessment of neurodegenerative disease. Neurotherapeutics. 14, 91–106. https://doi.org/10.1007/s13311-016-0487-6.
Vucic, S., Nicholson, G.A., Kiernan, M.C., 2008. Cortical hyperexcitability may precede the onset of familial amyotrophic lateral sclerosis. Brain. 131, 1540–1550. https://doi.org/10.1093/brain/awn071.
Wagnon, J.L., Barker, B.S., Hounshell, J.A., Haaxma, C.A., Shealy, A., Moss, T., Parikh, S., Messer, R.D., Patel, M.K., Meisler, M.H., 2016. Pathogenic mechanism of recurrent mutations of SCN8A in epileptic encephalopathy. Ann. Clin. Transl. Neurol. 3, 114–123. https://doi.org/10.1002/acn3.276.
Wainger, B.J., Kiskinis, E., Mellin, C., Wiskow, O., Han, S.S., Sandoe, J., Perez, N.P., Williams, L.A., Lee, S., Boulting, G., Berry, J.D., Brown Jr., R.H., Cudkowicz, M.E., Bean, B.P., Eggan, K., Woolf, C.J., 2014. Intrinsic membrane hyperexcitability of amyotrophic lateral sclerosis patient-derived motor neurons. Cell Rep. 7, 1–11. https://doi.org/10.1016/j.celrep.2014.03.019.
Weydt, P., Hong, S.Y., Kliot, M., Moller, T., 2003. Assessing disease onset and progression in the SOD1 mouse model of ALS. Neuroreport. 14, 1051–1054. https://doi.org/10.1097/01.wnr.0000073685.00308.89.
Williams, K.L., Fifita, J.A., Vucic, S., Durnall, J.C., Kiernan, M.C., Blair, I.P., Nicholson, G.A., 2013. Pathophysiological insights into ALS with C9ORF72 expansions. J. Neurol. Neurosurg. Psychiatry 84, 931–935. https://doi.org/10.1136/jnnp-2012-304529.
Wong, J.C., Makinson, C.D., Lamar, T., Cheng, Q., Wingard, J.C., Terwilliger, E.F., Escayg, A., 2018. Selective targeting of Scn8a prevents seizure development in a mouse model of mesial temporal lobe epilepsy. Sci. Rep. 8, 126. https://doi.org/10.1038/s41598-017-17786-0.
Wu, N., Enomoto, A., Tanaka, S., Hsiao, C.F., Nykamp, D.Q., Izhikevich, E., Chandler, S.H., 2005. Persistent sodium currents in mesencephalic v neurons participate in burst generation and control of membrane excitability. J. Neurophysiol. 93, 2710–2722. https://doi.org/10.1152/jn.00636.2004.
Yoshimura, T., Rasband, M.N., 2014. Axon initial segments: diverse and dynamic neuronal compartments. Curr. Opin. Neurobiol. 27, 96–102. https://doi.org/10.1016/j.conb.2014.03.004.
Yue, C., Remy, S., Su, H., Beck, H., Yaari, Y., 2005. Proximal persistent Na+ channels drive spike afterdepolarizations and associated bursting in adult CA1 pyramidal cells. J. Neurosci. 25, 9704–9720. https://doi.org/10.1523/JNEUROSCI.1621-05.2005.
Zanette, G., Tamburin, S., Manganotti, P., Refatti, N., Forgione, A., Rizzuto, N., 2002. Different mechanisms contribute to motor cortex hyperexcitability in amyotrophic lateral sclerosis. Clin. Neurophysiol. 113, 1688–1697.
van Zundert, B., Peuscher, M.H., Hynynen, M., Chen, A., Neve, R.L., Brown Jr., R.H., Constantine-Paton, M., Bellingham, M.C., 2008. Neonatal neuronal circuitry shows hyperexcitable disturbance in a mouse model of the adult-onset neurodegenerative disease amyotrophic lateral sclerosis. J. Neurosci. 28, 10864–10874. https://doi.org/10.1523/JNEUROSCI.1340-08.2008.